Tectonophysics 774 (2020) 228274

Contents lists available at ScienceDirect

Tectonophysics

journal homepage: www.elsevier.com/locate/tecto

Multiscale spatial distribution of crustal seismic anisotropy beneath the northeastern margin of the Tibetan plateau and tectonic implications of the Haiyuan fault

Yu-tao Shi[a], Yuan Gao[a,c,*], Xu-zhang Shen[b], Kelly H. Liu[c]

[a] Key Laboratory of Earthquake Prediction, Institute of Earthquake Forecasting, China Earthquake Administration, Beijing 100036, China
[b] Sun Yat-Sen University, Guangzhou 528400, China
[c] Missouri University of Science and Technology, Rolla, MO 65409, USA

ARTICLE INFO

Keywords:
Crustal seismic anisotropy
Shear-wave splitting
NE margin of the Tibetan plateau
Haiyuan fault
Tectonic implications

ABSTRACT

The Haiyuan fault is a large strike-slip fault in the northeastern (NE) margin of the Tibetan plateau. Using new data recorded by a temporary seismic array, this study obtains crustal seismic anisotropy measurements in different scales across the Haiyuan fault by analyzing splitting of shear-waves from local earthquakes. Parameters of shear-wave splitting (SWS) indicate clear zoning characteristics in seismic anisotropy in the upper crust. The study area is divided into two different anisotropic subzones by the Haiyuan fault. The dominant orientation of fast polarizations is NNE or NE north of the faults and WNW to EW south of the fault. This pattern of spatial variation indicates the controlling impact of Haiyuan fault to observed seismic anisotropy. With a zone of dozens of kilometers from the Haiyuan fault, the dominant orientations of fast polarizations are WNW, generally coincidental with the strike of the Haiyuan fault except for several stations. It indicates that the influence of the fault on stress could reach to about 10 km from the fault distance. Spatial pattern of anisotropy indicates multiple effects by stress, faults and local tectonics. It suggests different anisotropic mechanisms including stress-induced anisotropy and tectonic (or structural) anisotropy. The dominant orientation of fast polarizations can indicate *in situ* maximum horizontal principal compressive stress although there is always influence of tectonics.

The normalized time-delays are higher around the Haiyuan fault than those away from the fault, suggesting stronger crustal seismic anisotropy in a narrow belt around the strike-slip fault zone. The SWS parameters suggest that the Haiyuan fault is the actual crustal boundary of NE Tibetan plateau, about 200 km north of the reported boundary of the Tibetan plateau block. Combining with other studies in the crust and the lithosphere, this paper infers possible two-layer crustal anisotropy beneath the Yinchuan graben, north of the Haiyuan fault. The dominant orientation of fast polarizations are NNE or NE in the upper crust, probably originated from crack-induced anisotropy, but become WNW or NW in the middle-lower crust, possibly originated from deformation anisotropy.

1. Introduction

The Haiyuan fault is a strike-slip fault located in the northeastern (NE) margin of the Tibetan plateau and is surrounded by the Tibetan plateau, the South China block and two secondary blocks, the Ordos block and the Alxa block (Fig. 1). As one of the major faults in the boundary zone of the NE Tibetan plateau, the Haiyuan fault is the most dominant Cenozoic tectonic feature in the zone deformed by the extrusion of rigid blocks with large displacement and high slip rates (Meyer et al., 1998; Fan et al., 2004; Zheng et al., 2013; Wang et al., 2014; Shen et al., 2014, 2015). The arc-shaped Haiyuan fault belt consists of interrelated and independent secondary faults with multiple strands, which are referred to as the west segment and the east segment in this study, respectively (Fig. 1). The fault was interpreted as a belt of 250 m in width by fault-zone-trapped waves generated by near surface explosions (Liu et al., 2004). There are several internal pull-apart basins between these short fault segments (Burchfiel et al., 1991; Li et al., 2016). Due to the limited coverage of seismic stations around the Haiyuan fault, the fault characteristics, crustal structure, and lithospheric deformation beneath the boundary zone of the NE Tibetan

* Corresponding author at: Key Laboratory of Earthquake Prediction, Institute of Earthquake Forecasting, China Earthquake Administration, Beijing 100036, China
E-mail address: gaoyuan@cea-ies.ac.cn (Y. Gao).

https://doi.org/10.1016/j.tecto.2019.228274
Received 7 July 2019; Received in revised form 8 November 2019; Accepted 9 November 2019
Available online 18 November 2019
0040-1951/

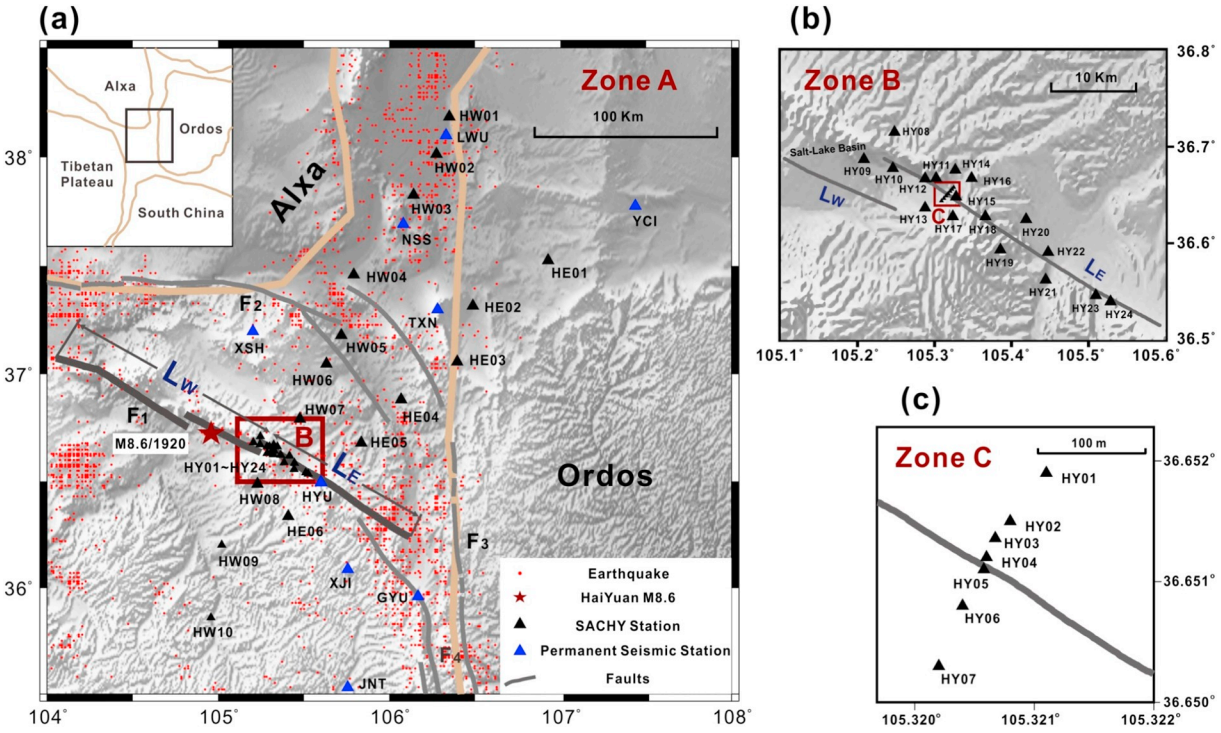

Fig. 1. Tectonic settings and seismic stations in the study area. The area divided by three zones in different ranges, *i.e.* (a) Zone A, (b) Zone B, and (c) Zone C. Black and blue triangles indicate the station locations of SACHY and regional seismic network, respectively. The earthy yellow lines denote boundaries of the major tectonic blocks (Deng et al., 2003). The red dots in zone A are local earthquakes from 1 Jan 2010 to 31 Dec 2017. The dark red star indicates the Haiyuan Ms8.6 earthquake in 1920. The small inset outlines the location of the study area. The dark brown frame in zone A outlines the locate of zone B, where black triangles indicate the location of the 24 seismic stations. L_W and L_E are the west and east segment of the Haiyuan fault. The dark brown frame in Zone B outlines the location of zone C, where black triangles indicate the location of the mini sub-array of 7 seismic stations. The gray lines are faults. F_1: Haiyuan fault; F_2: Tianjinshan fault; F_3: Yantongshan fault. F_4: Liupanshan fault. Alxa: Alxa block. Ordos: Ordos block. YG: Yinchuan Graben.

plateau remain ambiguous.

In the study area, numerous geophysical and geological studies have been conducted to investigate the regional stress field (Zhang et al., 2012a), upper-mantle anisotropy and dynamics (Chen et al., 2009; Li et al., 2011; Wang et al., 2013), regional tectonic conditions (Zhang et al., 2005, 2006), kinematics and geometries of the active faults (Yin et al., 2002; Wang et al., 2012; Gao et al., 2013), lithospheric structures (Wu et al., 2005; Pan and Niu, 2011; Chen et al., 2010; Shen et al., 2011; Tian and Zhang, 2013; Ye et al., 2015; Wang et al., 2017), and tectonic evolutions (Burchfiel et al., 1991; Song et al., 2001; Yin et al., 2008; Tian et al., 2014). GPS measurements show that the maximum principal strain is northeastward, consistent with the direction of the extrusion between the Indian plate and the Russia-Siberia platform (Wang et al., 2014; Shen et al., 2001; Gan et al., 2007). *In situ* stress measurements and focal mechanism solutions indicate that the orientation of the maximum dominant horizontal compressive stress in the NE Tibetan plateau is nearly northeastward (Xu, 2001; Sheng et al., 2015). While these studies have provided important constraints on the tectonic evolution models of the NE Tibetan plateau, detailed studies on the intra-continental crustal deformation, the related local stress conditions, and the influence of faults in the boundary zone of the NE Tibetan plateau are still lacking.

Seismic anisotropy is a ubiquitous property of the Earth's crust and upper mantle. Therefore, probing seismic anisotropy, which is quantified by the fast polarization orientation and the time delay of slow shear-wave (*i.e.* the splitting time), is an effective and commonly used technique in the study of crustal and mantle deformation. The two splitting parameters are very sensitive to fault geometry and properties (Gao et al., 1998, 2011; Gao and Crampin, 2004; Cochran et al., 2006). Based on the formation mechanisms, anisotropy in the upper crust can be divided into stress-induced anisotropy and structure-induced anisotropy (Crampin, 1977, 1981; Boness and Zoback, 2006a; Johnson et al., 2011; Li and Peng, 2017a). Stress-induced anisotropy is related to the alignment of microcracks in response to *in situ* stress field, that is, vertically stress-induced extensive-dilatancy anisotropy (EDA) microcracks (Crampin, 1981; Crampin and Peacock, 2005). Structure-induced anisotropy is associated with aligned planar features (Müller, 1991) such as sedimentary bedding planes (Leary et al., 1990) and aligned minerals or fabrics in the rock (Kern and Wenk, 1990; Lloyd et al., 2009), and sometimes controlled by faults (Crampin et al., 2002; Cochran et al., 2006; Gao et al., 2011). Stress-induced anisotropy in the upper crust is mostly attributed to local dominant compressive stress (Kaneshima, 1990; Gao et al., 1998, 2011; Wu et al., 2009; Shi et al., 2009, 2013; Kaviris et al., 2018; Crampin and Gao, 2018), and structure-induced anisotropy is widely observed in fault-zones (Boness and Zoback, 2006a, 2006b; Müller, 1991; Zinke and Zoback, 2000). Generally, vertically EDA microcracks in the crust tend to align parallel to the direction of compressive stress.

Shear-wave splitting (SWS) study in the vicinity of faults can reveal the influence of stress on the faults (Mizuno et al., 2005). Large faults are always associated with damaged rocks within the fault zone and surrounding areas. Moreover, upper crustal anisotropy measurement at densely spaced station measurements in the vicinity of active faults indicates spatial and temporal variations in the splitting parameters, such as those observed along the North Anatolian fault and the San Andreas fault (Peng and Ben-Zion, 2004; Boness, 2004; Boness and Zoback, 2006a, 2006b; Cochran et al., 2003, 2006; Liu et al., 2008).

In order to better resolve the spatial distribution of upper crustal anisotropy along and across the Haiyuan fault, we use a unique data set recorded by a dense seismic array to study the relationship between the spatial distribution of seismic anisotropy and active faults, as well as the tectonic implications of the Haiyuan fault in the NE margin of the

Tibetan plateau.

2. Data and analysis

Data used in the study were recorded by a dense temporary seismic array, the Seismic Arrays Cross the HaiYuan fault (SACHY), which was deployed for a two-year period from November 2012 to October 2014 by the Institute of Earthquake Science (presently the Institute of Earthquake Forecasting), China Earthquake Administration (Fig. 1). The SACHY consisted of 40 seismic stations that were deployed along two NE-SW oriented profiles, a fault-parallel dense array (oriented NW-SE), and a mini fault-perpendicular very dense sub-array (oriented NE-SW). The two NE-SW profiles, Haiyuan East (HE), and Haiyuan West (HW), are approximately perpendicular to the Haiyuan fault. Profile HE consisted of 10 stations equipped with Nanometrics observation systems, and HW had 6 Guralp CMG-3T stations. The fault parallel dense array of 17 stations was equipped with Guralp CMG-40T and CMG-3T seismometers, with a station interval of 1–3 km. The very dense fault-perpendicular array (*i.e.*, mini sub-array) had 7 stations with a station interval of 10 to 100 m, which seismometers are also Guralp CMG-40T. The array configuration of SACHY provides an excellent opportunity to study the spatial distributions and near-fault patterns of seismic anisotropy in the vicinity of an active fault.

To further improve the spatial coverage of the seismic stations, we also utilized data from 9 permanent seismic stations belonging to regional seismic networks from January 2010 to September 2017 in the study area, including 8 broadband stations of the Ningxia Provincial Seismic Network and one broadband station of the Gansu Provincial Seismic Network. The sampling frequency of all the waveform records is 100 samples per second. Small earthquake events were selected with magnitudes less than M_L3.5 in the earthquake catalogue of the China Earthquake Network Center.

In order to minimize the S-to-P converted phases which can distort the shear-wave waveform, seismic rays from small earthquakes to stations need to be within the shear-wave window, which is defined by an incidence angle of about 45° (Crampin and Peacock, 2005). The depths of seismic sources are larger than or equal to 5 km in order to reduce the influence of complex shallow crustal structure. High quality seismic waves from events within the shear wave window are filtered in the frequency range of 0.5 to 10 Hz to calculate anisotropic splitting parameters by a systematic analysis method of SWS, *i.e.*, SAM technology (Gao et al., 2008). This SWS analysis technique includes three aspects, the calculation of cross-correlation function, the elimination of time-delay, and the verification of polarization analysis (Gao et al., 1998, 2011; Shi et al., 2009). Figs. 2 and 3 show examples of SWS data analysis to obtain the splitting parameters.

3. Seismic anisotropy in the upper crust by shear-wave splitting

A total of 235 SWS measurements were obtained at 34 temporary seismic stations of SACHY, and 8 permanent seismic stations (Table 1). The mean value and the error of the fast polarization at each station were calculated by circular statistics (Berens, 2009). The majority of the stations show consistent measurements, although large scatters appear at a few stations (*e.g.*, HW08). The scatterness possibly suggests the complexity of local geologic structure, influence of irregular topography (Gao and Crampin, 2006; Gao et al., 2018).

Due to limited SWS measurements at some of stations, it is hard to accurately discuss the seismic anisotropy in these stations, such as stations JNT, XJI and TXN with one SWS result. But all SWS data are effective to the zonal anisotropic analysis. Based on the spatial coverage of the station, we divide the measurements into three zones. In zone A (the whole study area), the SWS parameters measured by the A-LR dataset (in a large range/scale for the whole study area) consisting of 98 records were obtained at 19 stations, including 11 SACHY and 8 permanent stations (Fig. 4). Results show obvious consistency in the fast polarizations, but variations in different regions. The average fast polarizations and average normalized time-delay is 58.5° ± 43.7° and 3.4 ± 1.9 ms/km, respectively (Fig. 4 and Table 2). The dominant orientations of fast polarizations at stations located north of the Haiyuan fault, including stations HW01–07, HE02–03, LUW, TXN, NSS, and XSH, are generally NNE, although some stations show NE or NS directions, which are sub-parallel to the direction of regional maximum principal compressive stress. However, dominant orientations of fast polarizations on the south of the Haiyuan fault, including stations HW08, HYU, XJI, GYU, and JNT, are nearly EW or WNW, reflecting the *in situ* maximum principal compressive stress. They are also approximately parallel to the strike of the Haiyuan fault, suggesting strong influence of the fault (Fig. 4). In addition, the fast polarizations at station HW08 seem to be in two dominant orientations, in NW and nearly EW (Fig. 4). This scatter pattern of fast polarizations suggests influence possibly from irregular topography (Gao and Crampin, 2006; Gao et al., 2011). The maximum principal compressive stress is nearly in WNW direction in the NE margin of the Tibetan plateau by the focal mechanism inversion (Bu et al., 2013; Xu et al., 2008; Wang et al., 2004; Sheng et al., 2015) and NNE direction between the Alex and Ordos blocks (Zhao and Liu, 1990; Zeng et al., 2015). The study area can be divided into different tectonic units on the basis of geological features, bounded by the Haiyuan fault (Burchfiel et al., 1991). Joint inversion of ambient noise tomography and receiver functions in NE boundary area of the Tibetan plateau suggests that seismic velocity structure exhibits prominent difference beneath the two sides of the Haiyuan fault at the depth of 15 km (Guo and Chen, 2017), and significantly different Vp and Vs beneath two sides of the Haiyuan fault at the depth from 5 to 20 km is also revealed (Xiao and Gao, 2017).

In zone B (the Haiyuan fault area), the SWS parameters measured by the B-HY dataset (in higher resolution around the Haiyuan fault) from 102 records were obtained at 17 stations. These stations are mainly around the L_E segment of the Haiyuan fault (Fig. 5). The fast polarizations of SWS are sub-parallel to the strike of the fault at both sides of the fault, although there are some differences at several seismic stations (Fig. 5). Generally, the WNW-oriented fast polarizations are parallel to the strike of the fault within 10 km from the fault itself. However fast polarizations of station HY09 at west end of the segment L_E show different dominant direction, almost perpendicular to the strike of the fault. Note station that HY09 is less than 4 km to the fault L_W and also at the end of L_E (Fig. 5). Measurements at this station may typically indicate the influence of the fault, since the end of fault changes the local stress field (Tai et al., 2009; Zhao et al., 2012; Shi et al., 2013). At another side, the apparently scattered fast polarizations at station HY13 to the end of the fault segment L_W possibly suggest the influences of the two fault segments (L_W and L_E). In addition, three stations HY17, HY18, and HY19 show different dominant directions of fast polarizations approximately in NW, which is consistent with the NW direction of the *in situ* maximum principal compressive stress in NW direction (Zhang et al., 2012a), different to most of stations. Station HY20 also shows different dominant directions of fast polarizations approximately in EW. The different fast polarizations at these four nearby stations may suggest variation of local stress field around the fault (Fig. 5).

The mean direction of fast polarizations in zone B is 111.5° ± 31.6° and the mean normalized time-delay is 3.7 ± 2.4 ms/km (Table 2). The mean directions of fast polarizations at most of stations are consistent, less than 20° from the strike of the fault, which preferentially exhibit parallel to the direction of maximum principal compressive stress (Crampin, 1981; Gao et al., 1998, 2011). The variations reveals complicated local stress pattern, *i.e.*, localization of stress field. However, the local structure and irregular topography may also induce scatter of fast polarizations (Gao and Crampin, 2006), such as stations HY11 and HY14.

In zone C (the mini profile), the SWS parameters measured by the C-MP dataset (in much higher resolution in dozens of meters around the fault) from 35 records were obtained at 7 stations from local

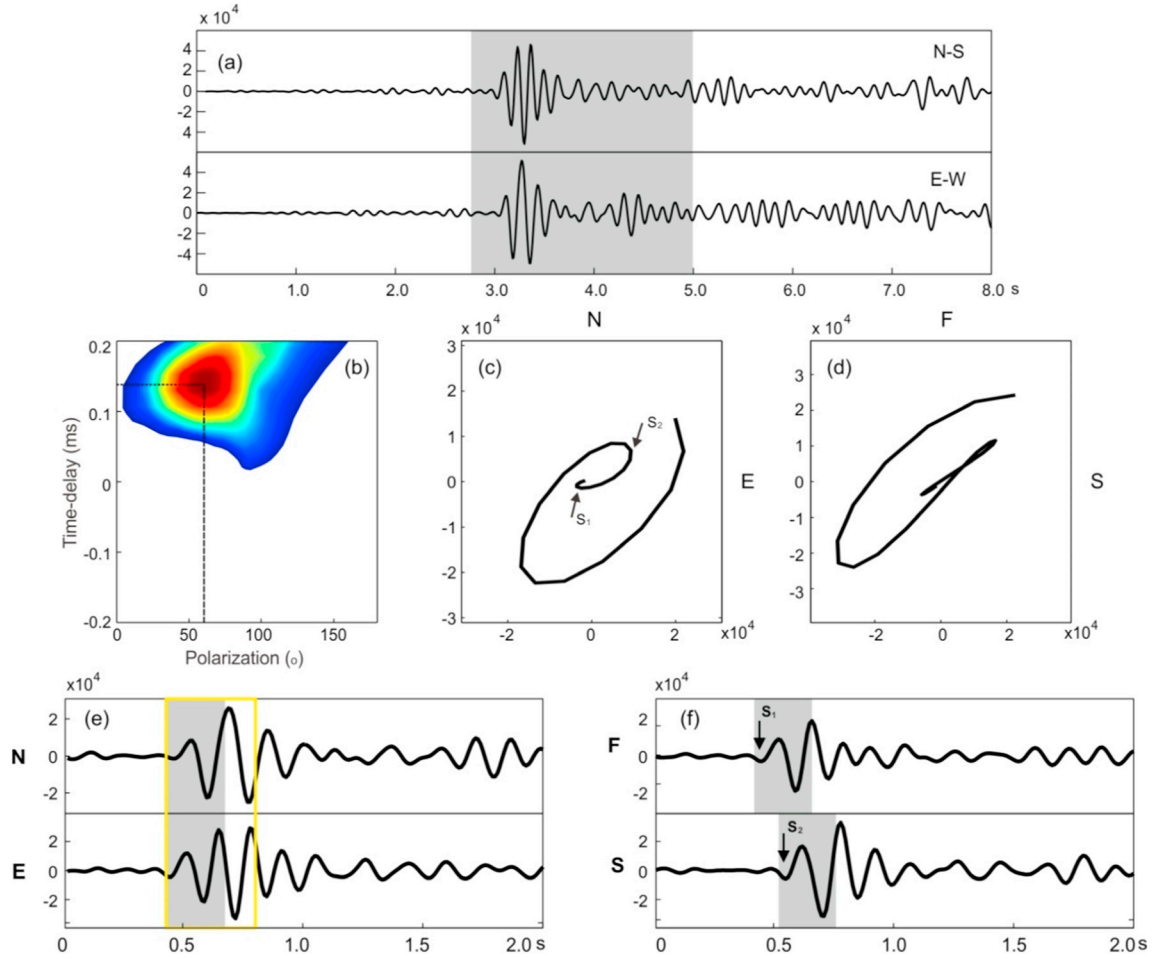

Fig. 2. An example of the shear-wave splitting analysis for the seismic event recorded at HY20. The event (M_L = 2.3) occurred at 08:53:19 on 2013/03/25 at depth of 5.0 km. (a) The original waveforms of north-south (NS) and east-west (EW) components. (b) The colorful contour map of cross-correlation function *vs.* different time-delay and polarization. The fast polarization and time-delay are separately 60° and 0.14 s. (c) The polarization diagram of shear-waves. S_1 means the fast shear-wave. S_2 means the slow shear-wave. (d) The polarization diagram of the fast shear-wave and the slow shear-wave after the effect of time-delay is eliminated. (e) The shear waveforms in NS and EW direction. After elimination of time-delay and verification of polarization, the fast polarization and time-delay are finally 60° and is 0.10 s. (f) The waveforms of the fast shear-wave (F) and the slow shear-wave (S). The ordinate is the count value of amplitude. The abscissa is the number of sampling points. The yellow frame of shear waveform is used to compute the cross-correlation function. The shade areas in (a) are enlarged in (e) and (f). The shade areas in (e) and (f) mark the segment of shear waveforms showed in polarization diagrams of (c) and (d), respectively. (For interpretation of the references to color in this figure legend, the reader is referred to the web version of this article.)

earthquakes in depths from 8 km to 13 km (Fig. 6). Dominant fast polarization orientations are generally parallel to the fault. The mean orientation of the fast polarizations is 138° ± 17.1°. However, stations HY02 and HY01 display different orientations of fast polarizations, although station (HY02) is only 50 m away from the fault (Fig. 6). The mean time-delay is 5.4 ± 2.5 ms/km, which is larger than those in zone B and zone A (Table 2).

Orientations of fast polarizations are parallel to alignment direction of stress-induced EDA microcracks and maximum horizontal principal compressive stress (Crampin, 1981; Crampin and Peacock, 2005; Gao et al., 1998; Kaviris et al., 2018) only if disturbance from tectonics or faults could be moved out (Gao et al., 2010, 2011). By average orientations of fast polarizations, we could extract orientations of regional maximum horizontal principal compressive stress (Fig. 7). Rose diagrams in different subzones indicate that dominant orientation of fast polarizations in the NE Tibetan plateau is to NNE or NE but with secondary dominant orientation to WNW nearly EW in the southern area and near the Haiyuan fault. The dominant orientation of fast polarizations around the Haiyuan fault is to WNW or NW (Fig. 9).

For time-delay of SWS, the most plausible explanation is the evolution of fluid-filled EDA cracks in the crust (Crampin and Zatsepin, 1997). In this study, the normalized time-delay varies greatly from 2.0 to 7.7 ms/km at station (rejecting single record) and shows the dispersion with high standard deviations (Fig. 10 and Tables 1 and 2). In zone A, the mean time-delay observed at stations in the region far away from the Haiyuan fault is 3.4 ± 1.9 ms/km, which is identical to previous results in larger area in the NE Tibetan plateau (Zhang et al., 2012a; Guo et al., 2015; Qian et al., 2017). In zone B, the mean normalized time-delay at the stations near the Haiyuan fault is 3.7 ± 2.4 ms/km, which is higher than that in zone A. Stations in zone A are much further from the fault than those in zone B. In zone C, the mean time-delay at the stations almost on the Haiyuan fault is 5.4 ± 2.5 ms/km, which is the highest.

4. Discussions

4.1. The zoning characteristics, complicated mechanisms and tectonic implications of seismic anisotropy

Seismic anisotropy, no matter whether it originates from aligned EDA microcracks, intrinsic rock type, or tectonic feature, is useful to describe local stress state and crustal seismic structure. In this study,

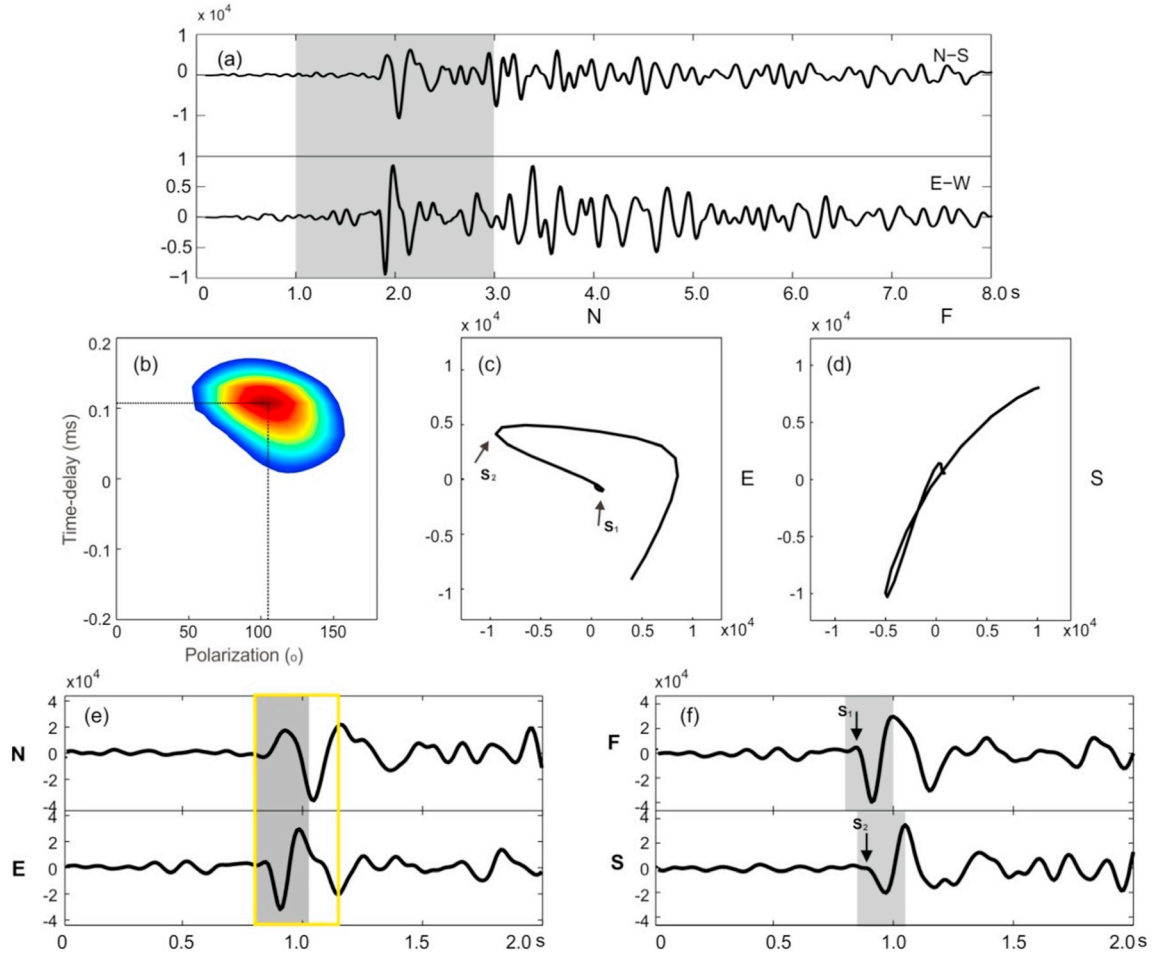

Fig. 3. An example of the shear-wave splitting analysis for the seismic event recorded at HY13. The event (M_L = 1.2) occurred at 15:09:47 on 2014/09/30 at a depth of 8.0 km. The fast polarization and time-delay are 105° and 0.11 s by calculation of cross-correlation. After elimination of time-delay and verification of polarization, the fast polarization and time-delay are finally 110° and is 0.06 s. Others notations are same as in Fig. 2.

Table 1
Parameters of seismic anisotropy in the upper crust[a].

Station	*N*	$\varphi \pm \delta\varphi$(°)	$t_n \pm \delta t_n$ (ms/km)	Station	*N*	$\varphi \pm \delta\varphi$(°)	$t_n \pm \delta t_n$ (ms/km)
HE02	2	15.0 ± 15.0	3.7 ± 0.2	HY12	7	120.8 ± 15.6	4.9 ± 2.6
HE03	5	59.8 ± 16.6	3.2 ± 0.8	HY13	8	118.6 ± 20.1	4.6 ± 2.5
HW01	3	163.3 ± 4.7	5.1 ± 2.5	HY14	9	103.4 ± 31.7	3.7 ± 2.3
HW02	8	42.5 ± 8.3	2.4 ± 1.6	HY15	7	134.3 ± 19.0	3.3 ± 1.7
HW03	8	23.8 ± 14.9	4.1 ± 1.9	HY16	4	120.0 ± 7.0	2.6 ± 0.4
HW04	4	37.5 ± 9.6	2.7 ± 1.2	HY17	7	153.7 ± 18.1	3.9 ± 2.0
HW05	8	37.7 ± 17.0	3.0 ± 1.4	HY18	3	140.1 ± 14.0	2.0 ± 1.6
HW06	3	166.2 ± 23.3	4.4 ± 2.9	HY19	5	150.0 ± 6.3	3.7 ± 1.7
HW07	2	30.0 ± 19.9	3.1 ± 0.7	HY20	8	78.8 ± 9.2	3.3 ± 1.1
HW08	2	155.0 ± 5.2	4.1 ± 1.4	HY21	4	115.1 ± 16.4	5.1 ± 2.1
	3	83.5 ± 17.2	3.5 ± 2.7	HY22	6	120.0 ± 8.2	4.6 ± 3.9
HY01	5	152.0 ± 7.5	3.6 ± 1.7	HY23	6	82.4 ± 14.5	4.1 ± 2.4
HY02	6	160.0 ± 8.2	4.0 ± 0.7	HY24	2	110.0 ± 10.0	4.0 ± 0.1
HY03	6	133.3 ± 13.7	6.0 ± 2.1	LWU	9	24.0 ± 4.9	5.4 ± 2.7
HY04	5	134.0 ± 4.9	5.1 ± 2.2	NSS	8	171.5 ± 18.7	5.3 ± 2.3
HY05	4	115.2 ± 14.9	5.6 ± 2.7	HYU	7	91.6 ± 13.2	7.0 ± 4.6
HY06	4	127.4 ± 14.7	7.7 ± 3.3	XJI	1	95.0	4.4
HY07	5	136.0 ± 4.9	6.3 ± 3.1	GYU	18	79.2 ± 29.1	6.0 ± 3.2
HY08	3	116.6 ± 9.41	4.1 ± 2.5	JNT	1	110	4.5
HY09	6	38.1 ± 15.6	2.2 ± 0.7	XSH	5	38.4 ± 18.7	3.3 ± 1.4
HY10	10	101.4 ± 21.0	3.6 ± 1.5	TXN	1	50	1.8
HY11	7	110.1 ± 21.0	3.3 ± 0.5				

[a] Note: *N* is the number of measurements. φ is the mean polarization direction, t_n is the mean normalized time-delay with corresponding standard errors ($\delta\varphi$ and δt_n).

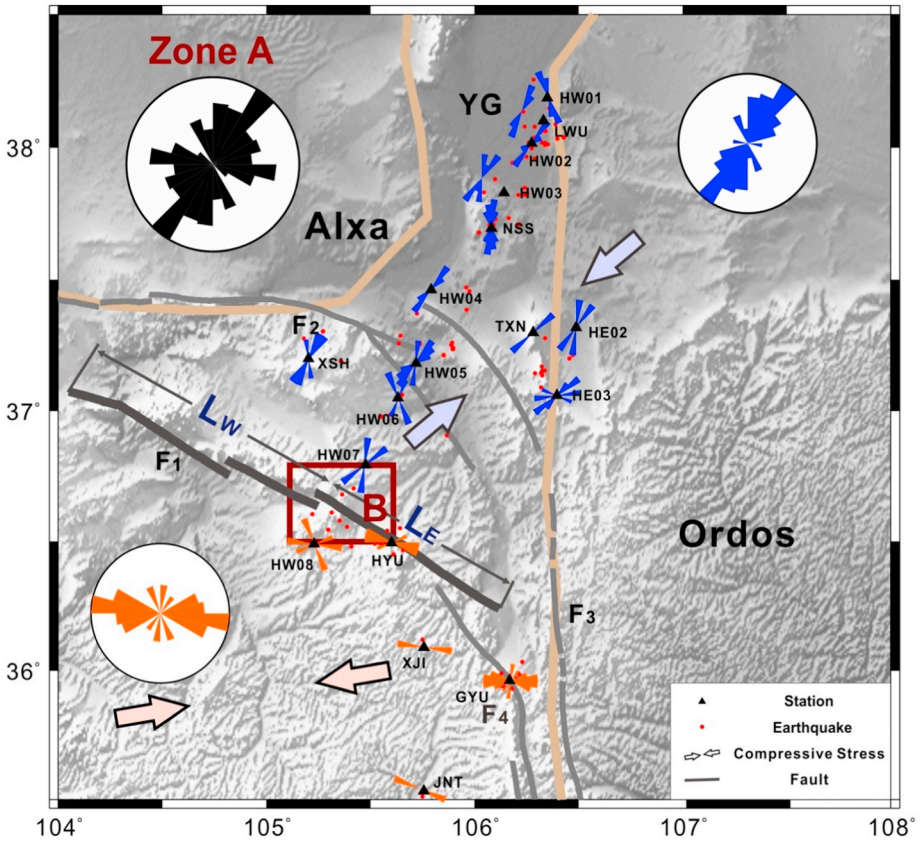

Fig. 4. Fast polarizations in the study area (zone A). Equal area project rose diagrams of fast polarizations are shown at each station in blue or in orange. The blue and orange circled equal area project rose diagrams are fast polarizations superimposed SWS data at stations separately on the both sides of Haiyuan fault. The black rose diagram depicts all SWS data in zone A. The red dots are the epicenters of events for SWS measurements in this study. Two pairs of arrows indicate maximum local horizontal principal compressive stress (Xu, 2001; Sheng et al., 2015). The dark brown bordered box outlines zone B. Note: the SWS data in zone A do not include those in zone B. (For interpretation of the references to color in this figure legend, the reader is referred to the web version of this article.)

Table 2
Parameters of seismic anisotropy in the different subzones[a].

Zone	*N*	$\varphi \pm \delta\varphi$ (°)	$t_n \pm \delta t_n$ (ms/km)
Zone A	98	58.5 ± 43.7	3.4 ± 1.9
Zone B	102	111.5 ± 31.6	3.7 ± 2.4
Zone C	35	138.4 ± 17.1	5.4 ± 2.5
Zone B + C	137	118.9 ± 30.7	4.2 ± 2.6
Zone A + B + C	73	34.9 ± 19.3	3.5 ± 2.3
	162	122.1 ± 26.5	4.7 ± 3.1

[a] Note: The SWS parameters in the zone A, B and C are independent.

seismic anisotropy in the upper crust was measured by SWS at 42 seismic stations from the temporary SACHY stations and permanent stations of regional seismic networks. The SACHY data provide with a good opportunity to study subtle variations of crustal seismic anisotropy around a large active fault in scale of meters. The SWS parameters obtained at the 42 stations clearly show spatial variations of crustal seismic anisotropy and suggest multiple induced mechanisms to observed anisotropy around the Haiyuan fault in the NE margin of the Tibetan plateau. By SWS measurements, arresting spatial variations both in the measured fast polarizations and time-delays reveal remarkable complexity of shear wave anisotropy in the crust beneath the NE margin of the Tibetan plateau. This study suggests that SWS parameters near the fault are heavily affected by the presence of fault and boundary of tectonic blocks.

Dominant orientation of fast polarizations is NNE in the area north of the Haiyuan fault and WNW nearly EW south of the fault (see the right diagram in Fig. 9). This result clearly indicates the influence of the Haiyuan fault on the observed seismic anisotropy at least in upper crust (Fig. 4). It also suggests that real boundary of the NE Tibetan plateau is the Haiyuan fault, which is about 200 km north of the boundary shown in Fig. 1, although the upper mantle of Tibetan plateau block is reported beyond the Haiyuan fault, about 100 km to the northeast (Shen et al., 2017).

With more SWS data by Zhang and Gao (2017), Fig. 7 shows that at a distance of about 20 km east of mini sub-array (Fig. 6), trapped waves suggest a fault width of about 250 m (Liu et al., 2004). Based on the pattern of fast polarizations in zone B and zone A, the anisotropic sources are possibly different. On the fault or in the neighboring area within 10 km to the fault, the fault possibly controls (or strongly influences) the pattern of seismic anisotropy in the upper crust. Influences of local stress on anisotropy always mix with those of tectonics, maybe as well as structural impact. The measurements of seismic anisotropy in the study area indicate different anisotropic mechanisms, which include some simultaneous effects by stress, tectonic (or structural) impact and even intrinsic rock type. Some studies reported tectonic (or structural) impacts to seismic anisotropy in the crust (Gao et al., 2011, 2018; Li and Peng, 2017b). However, the dominant orientation of fast polarizations could indicate orientation of *in situ* maximum horizontal principal compressive stress, only if disturbance from tectonics or fault effects can be ruled out (Gao et al., 2011, 2018).

Based on the time-delay measurements, normalized time-delays at stations around the Haiyuan fault show generally higher values than those far away the faults (Fig. 10). Time-delay of SWS is related to the degree of seismic anisotropy. It suggests that crustal seismic anisotropy in a narrow belt around and along a large strike-slip fault zone could be stronger than areas far away from the fault zone.

Previous study on the San Andreas Fault suggested that the 5 km is the minimum distance to distinguish the structural anisotropy and stress-induced anisotropy (Boness and Zoback, 2006a, 2006b). The fast polarization of crustal SWS reveals that the stress-induced anisotropy dominates the area far from the active fault, and more complicated anisotropy near the fault is mixed with stress-induced and structural (or tectonic) anisotropy.

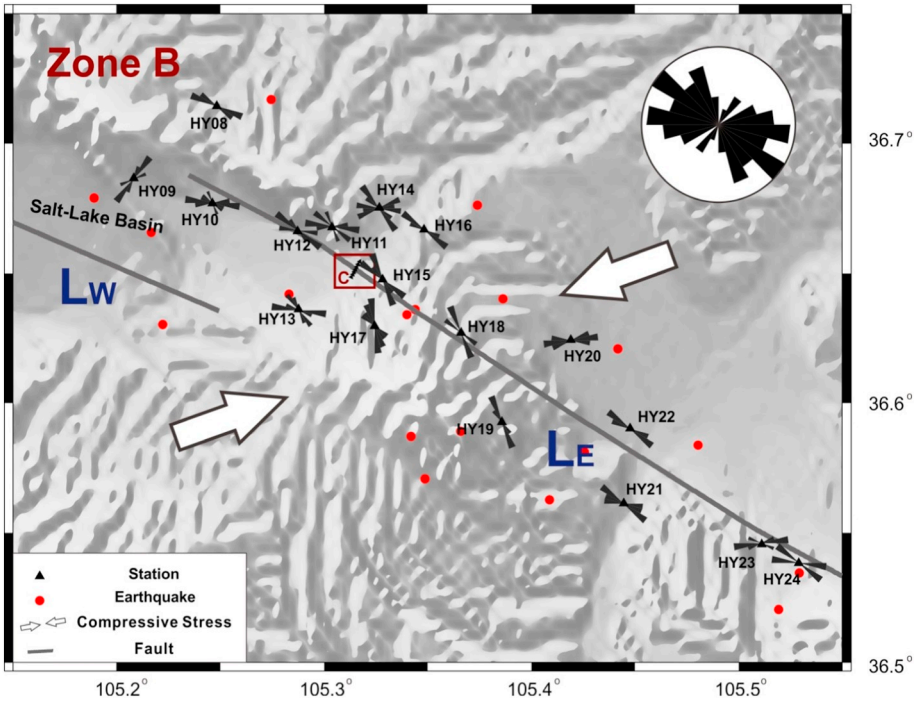

Fig. 5. Fast polarizations in zone B. There are 17 seismic stations (HY08~HY24) shown available SWS data. The black circled equal area project rose diagrams at the top-right are fast polarizations superimposed SWS data from all 17 stations. The dark brown bordered box marked C outlines the area in Fig. 6. A pair of white arrows indicates maximum local horizontal principal compressive stress along the Haiyuan Fault zone (from Shi et al., 2013). The red dots indicate the epicenters of events for SWS in this study. Note: the SWS data in zone B do not include those in zone C. Other notations are same as in Fig. 4. (For interpretation of the references to color in this figure legend, the reader is referred to the web version of this article.)

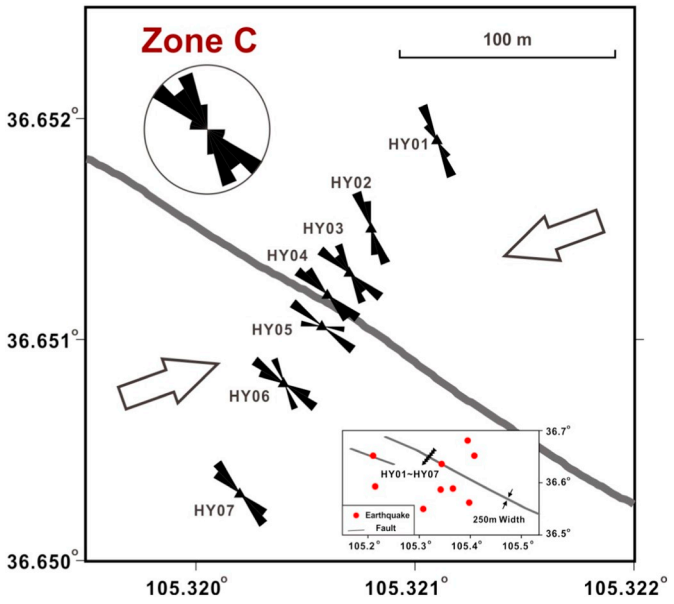

Fig. 6. Fast polarizations in zone C. There are 7 seismic stations (HY01–HY07) in this mini seismic sub-array. The black circled equal area project rose diagrams at the top-left are fast polarizations superimposed SWS data from all 7 stations. In the bottom inset, red dots indicate epicenters of events for SWS measurements in this study and a pair of arrows indicate the measurement position for the trapped wave of the fault zone (Liu et al., 2004), about 20 km east to the mini sub-array. (For interpretation of the references to color in this figure legend, the reader is referred to the web version of this article.)

4.2. Influence range of the Haiyuan fault on seismic anisotropy and the striking change of seismic anisotropy

In the narrow zone around the Haiyuan fault, the fast orientations from the B-HY stations are mostly WNW, generally consistent with the strike of the Haiyuan fault (Fig. 5). Obvious local changes of fast polarizations exist at several stations, such as station HY09, which indicate different orientation of *in situ* maximum principal compressive stress. It may also indicate the effect of combined action from faults and disturbed regional background stress field. Some stations may be influenced by fault and local tectonic feature, such as stations HY17-20. This kind of combined action results in a local stress that is different from other area. It suggests that the influence of fault may extend to further distance, at least 10 km from the fault.

The fast orientations at the C-MP stations are consistent with the strike of the Haiyuan fault. For example, the dominant orientations of fast polarizations are perfectly parallel to the fault at stations HY03-07 (Fig. 6). This fault parallel pattern is consistent with earlier studies in other regions (Cochran et al., 2006; Gao et al., 2011; Li and Peng, 2017a). Dominant orientations of fast polarizations change slightly at stations HY01 and HY02, suggesting that the dominant orientation of fast polarizations will possibly show some variations if the station is beyond 100 m from the fault.

SKS, SKKS and PKS (called XKS later) splitting measurements in the NE margin of the Tibetan plateau show WNW-ESE fast orientations, which are roughly parallel to the strike of the major faults, suggesting that lithospheric anisotropy is associated with the present-day orogeny (Li et al., 2011; Zhang et al., 2012b; Wang et al., 2013; Ye et al., 2016; Huang et al., 2017). The spatial distribution of the observed seismic anisotropy from XKS splitting indicates that the Haiyuan fault also plays an important role in the process of lithospheric deformation, probably related to lithosphere underthrusting by the Alax block (Zhang et al., 2012b; Ye et al., 2016).

In the NE margin of the Tibetan plateau, lots of previous studies on Moho depths using receiver functions and seismic profiles claimed that the Moho depths vary from thicker in the southwest part to thinner in the northeast part, and abruptly jumps beneath the Haiyuan fault (Zhang et al., 2011; Pan and Niu, 2011; Ye et al., 2015). This suggests the Haiyuan fault is a deep large fault which breaks the crust and reaches to the topmost of the upper mantle. The SWS data in this study indicate that the Haiyuan fault is a clear boundary between the north subzones and the south subzones.

4.3. Layered seismic anisotropy in the NE margin of the Tibetan plateau

Moho Ps splitting observations suggest that the mid-lower crustal anisotropy has a WNW-ESE polarization (Wang et al., 2016; Xu et al.,

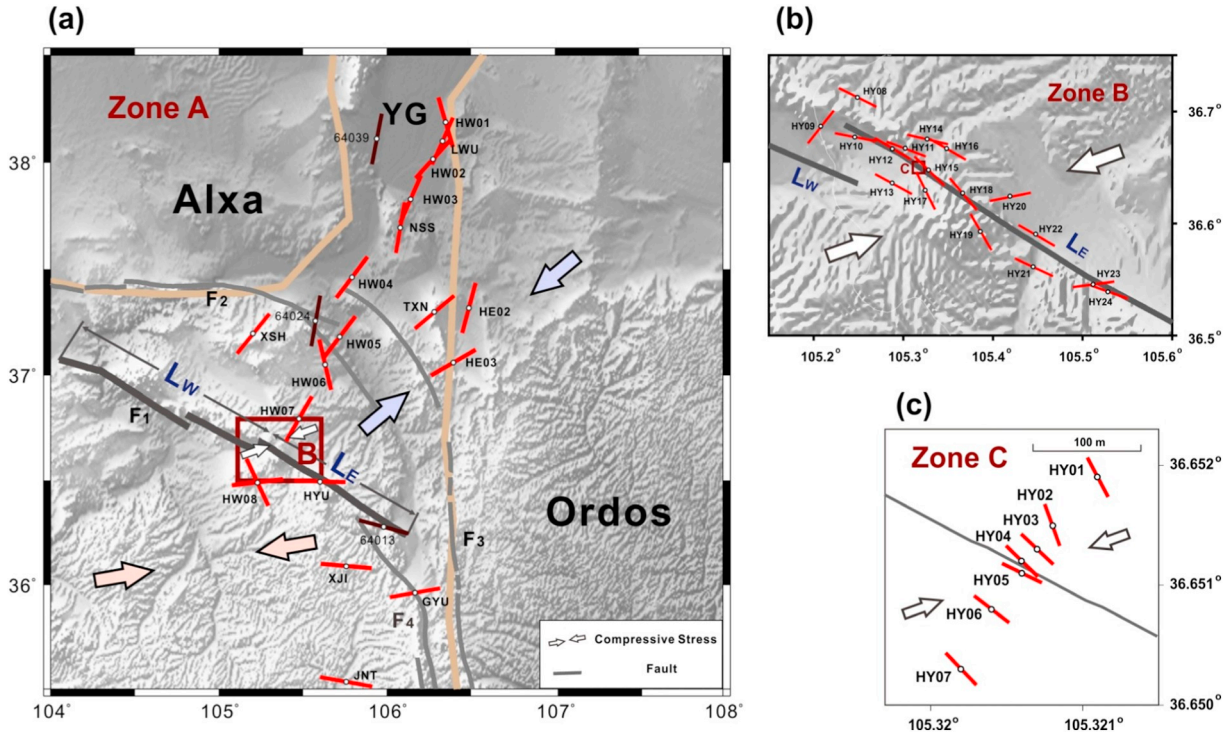

Fig. 7. Distribution of average fast polarizations in the study area. Red bars indicate the mean fast polarizations. Dark bars are data from Zhang and Gao (2017). (For interpretation of the references to color in this figure legend, the reader is referred to the web version of this article.)

2018; Guo et al., 2019). The consistency among the fast orientations from local S, Moho Ps, and XKS splitting suggests consistent anisotropic parameters from the entire crust and upper mantle, and implies a vertically coherent deformation over the entire lithosphere beneath the Haiyuan fault (Wang et al., 2013, 2016; Wu et al., 2015; Xu et al., 2018; Guo et al., 2019). The fast polarizations in the upper crust by SWS of local data are consistent with the principal compression in NE direction revealed by GPS data (Chen et al., 2004; Gan et al., 2007), nearly perpendicular to those in the mid-lower crust (Li et al., 2011; Zhang et al., 2012a; Wang et al., 2016). The radial anisotropy in the crust by ambient noise tomography also indicated different anisotropic patterns between the upper crust and the mid-lower crust in the NE Tibetan plateau (Tan et al., 2015). This difference suggests that the mechanism of seismic anisotropy in the upper crust is different from that in the mid-lower crust.

Due to the lateral flow in the lower crust caused by the collision between the Indian and Eurasian plates, it has been proposed that the sub-horizontal alignments of anisotropic minerals are closely related to the mid-lower crustal anisotropy in the NE Tibetan plateau (Shapiro et al., 2004; Tan et al., 2015; Ye et al., 2016). The WNW fast orientation possibly originates from the middle and low crust by Ps data (Wang et al., 2016). A thin low velocity zone has been observed in the middle crust (Ye et al., 2015; Li et al., 2017), which is associated with crustal decoupling deformation. This observation indicates that deformation decoupling may exist in the crust beneath the NE margin of the Tibetan plateau, where the decoupling depth is possibly at the bottom of the upper crust. We speculate that stress-induced cracks are the main anisotropy forming mechanism for the upper crust, and alignments of anisotropic minerals are the main cause for the mid-lower crust anisotropy (Fig. 8). Moreover, this study infers that two-layer crustal anisotropy possibly exists beneath the NE margin of the Tibetan plateau, from the north of Haiyuan fault to the south part of the Yinchuan graben (Fig. 8), with NNE fast polarizations in the upper crust and WNW direction in the mid-lower crust.

5. Conclusions

By the elaborate temporary seismic arrays SACHY, using more seismic stations than previous studies, this study obtains upper crustal seismic anisotropy beneath the NE margin of the Tibetan plateau from regional scale (~10^4 m), local scale (~10^3 m) to fine scale (~10^1 m). SACHY traversed the strike-slip Haiyuan fault and consisted of three seismic sub-arrays with different observation aperture. Using recording of small local earthquakes at 40 SACHY stations plus 8 permanent seismic stations, we acquire spatial patterns of seismic anisotropy in the upper crust across the Haiyuan fault. It is the first time to detect finer seismic anisotropy in the upper crust in multiscale around the Haiyuan fault and to discuss its tectonic implications in view of seismic anisotropy.

In the NE margin of the Tibetan plateau, seismic anisotropy in the upper crust is divided into two subzones by the Haiyuan fault. General pattern shows two dominant orientations of fast polarizations in entire study area. However it is clear the dominant orientation of fast polarizations is in NNE direction in north of the Haiyuan fault and WNW nearly NW in south of the Haiyuan fault. It indicates the controlling impact of the Haiyuan fault on seismic anisotropy at least in the upper crust.

Around the Haiyuan fault, the dominant orientations of fast polarizations are WNW, generally coincidental with the strike of the Haiyuan fault in a scale of dozens of kilometers. Fast polarizations at some stations show obvious different local changes, indicating variation of *in situ* compressive stress. It indicates multiple effect of combined action by stress, faults and local tectonics, suggesting influence of the Haiyuan fault on the stress field could reach to about 10 km of station-to-fault distance. However, fast polarizations perfectly parallel to strike of the strike-slip fault could be within 100 m to the Haiyuan fault, which is similar to other SWS studies on the strike-slip fault. It suggests that the Haiyuan fault is the actual crustal boundary of the NE Tibetan plateau, which is about 200 km north of the reported boundary of the Tibetan plateau block. The normalized time-delays are higher around the Haiyuan fault than areas away from the fault, suggesting stronger

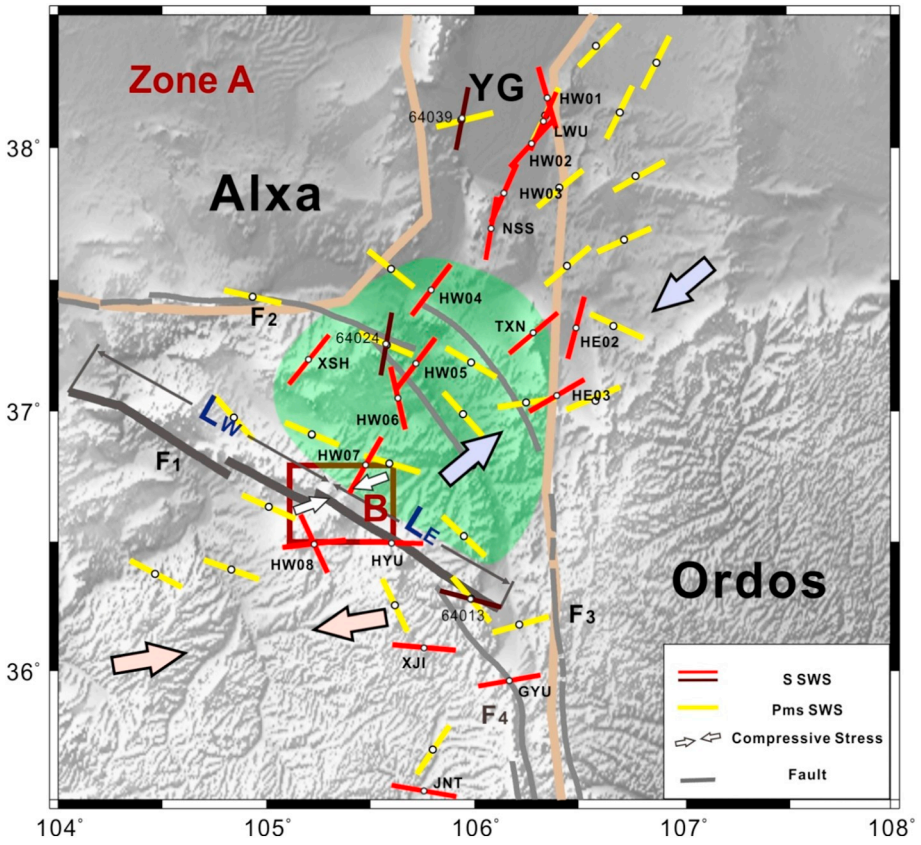

Fig. 8. Average fast polarizations of local SWS (red and dark bars, same as in Fig. 7) and Moho Ps splitting (yellow bars) in the study area. Moho Ps data are from Xu et al. (2018). The green shaded area is inferred the two-layer crust anisotropy. (For interpretation of the references to color in this figure legend, the reader is referred to the web version of this article.)

crustal seismic anisotropy in a narrow belt around the strike-slip Haiyuan fault than far from the fault.

This study suggests different anisotropic mechanisms in the study area. Crustal anisotropy could be influenced in some simultaneous effects by stress, intrinsic rock type, tectonic or structural impact, possibly in the area of about 10 km to the fault. Presently it is difficult to accurately identify and separate multiple effects from stress-induced EDA microcracks or structural (or tectonic) factors. The dominant orientations of fast polarizations can always indicate *in situ* maximum principal compressive stress, although there is also disturbance from structural anisotropy. This study suggests that stress-induced microcracks are the main cause of the upper crustal anisotropy, although mixed with tectonic anisotropy (or structural anisotropy). Although it is still a problem to recognize or separate different anisotropic source in the crust, this study opens a window to detect complicated mechanisms and laminarity of seismic anisotropy.

Based on splitting measurements of local S, Moho Ps and XKS phases, combining with discussions on seismic structure and anisotropy in mid-lower crust, this study infers the two-layer crustal anisotropy beneath the NE margin of the Tibetan plateau, from the south part of the Yinchuan graben to the north of the Haiyuan fault. The dominant orientation of fast polarizations are NNE or NE in the upper crust originated from crack-induced anisotropy, but WNW or NW in the middle-lower crust possibly originated from deformation anisotropy.

Depth of seismic anisotropy in the crust is difficult to be accurately identified by SWS since lack of data. Seismic anisotropy in shallow layer 1 or 2 km in the topmost crust is often overlapped by effects of crack-induced anisotropy and structural anisotropy, which could not be separated well effectively. However more data with excellent depth range is helpful to determine depth distribution of seismic anisotropy.

Acknowledgements

This work is supported by NSFC Project 41474032 and the Basic Research Project of the Institute of Earthquake Forecasting, China Earthquake Administration (2012IES010101). We are grateful to Drs. Weijun Wang, Ning Liu, Anhui Sun, and the field work team for their supports in the deployment temporary seismic stations. We thank Ms.

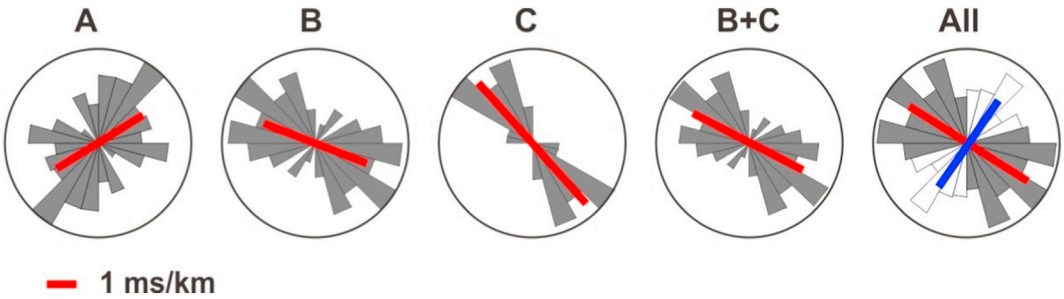

Fig. 9. The equal area project rose diagrams of fast polarizations in different subzones. The circled rose diagrams from the left to the right, marked A, B, C, B + C and All, which stand for SWS data in zone A, zone B, zone C, zone B plus C, and the entire data in the study area, respectively. Red and blue bars indicate the mean fast polarizations and mean time-delays. (For interpretation of the references to color in this figure legend, the reader is referred to the web version of this article.)

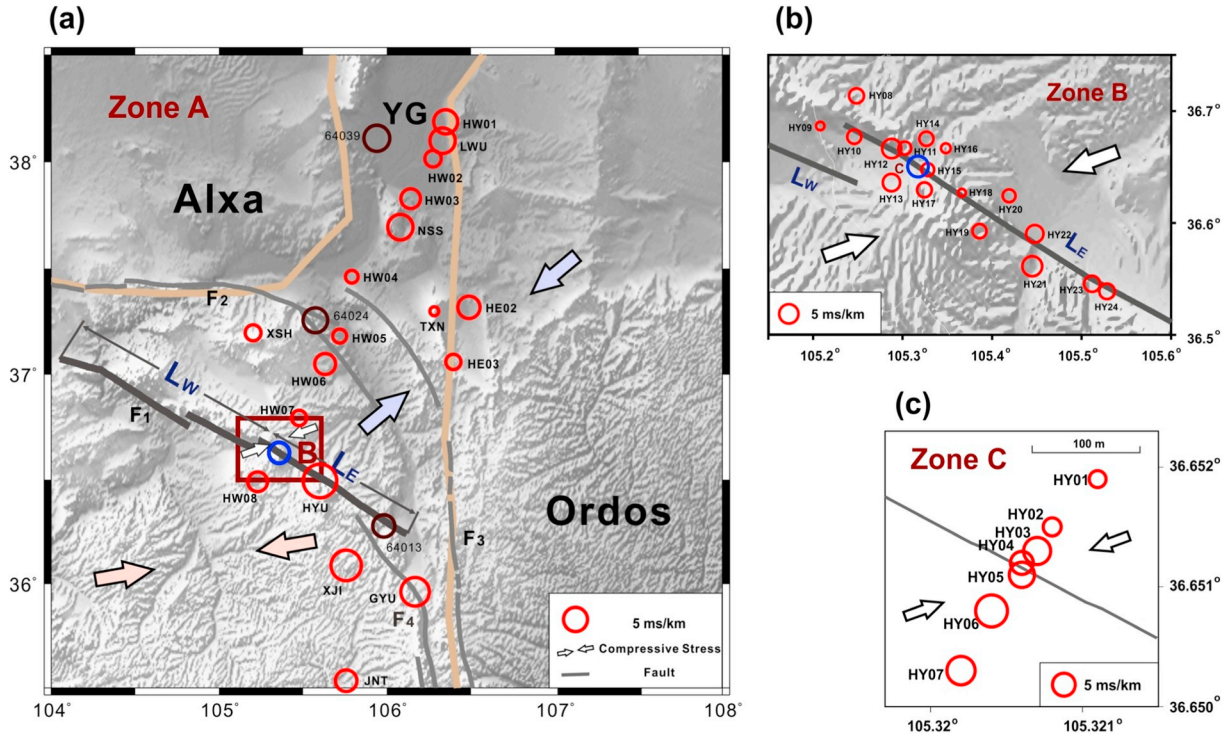

Fig. 10. Distribution of average normalized time-delays in the study area. Red circles indicate the time-delay. The blue circle in (a) indicate the mean time-delays of the B-HY dataset in zone B. The blue circle in (b) indicate the mean time-delays of the C-MP dataset in zone C. (For interpretation of the references to color in this figure legend, the reader is referred to the web version of this article.)

Lingxue Tai and Ms. Yi Zhang for their partly assistance in SWS data processing and discussions. We appreciate helpful comments and suggestions from the editor and two reviewers to improve this paper.

References

Berens, P., 2009. CircStat: a MATLAB toolbox for circular statistics. J. Stat. Softw. 31 (10). https://doi.org/10.18637/jss.v031.i10.

Boness, N.L., 2004. Stress-induced seismic velocity anisotropy and physical properties in the SAFOD Pilot Hole in Parkfield, CA. Geophys. Res. Lett. 31 (15), L15S17.

Boness, N.L., Zoback, M.D., 2006a. A multiscale study of the mechanisms controlling shear velocity anisotropy in the San Andreas Fault Observatory at Depth. Geophysics 71 (5), 131–146.

Boness, N.L., Zoback, M.D., 2006b. Mapping stress and structurally controlled crustal shear velocity anisotropy in California. Geology 34 (10), 825–828.

Bu, Y.F., Wan, Y.G., Zhang, Y.S., 2013. Tectonic stress analysis in Gansu and its adjacent areas. Seismology and Geology (Chinese Edition) 35 (4), 833–841.

Burchfiel, B.C., Zhang, P., Wang, Y., Zhang, W., Song, F., Deng, Q., Peter, M., Leigh, R., 1991. Geology of the Haiyuan fault zone, Ningxia-hui autonomous region, China, and its relation to the evolution of the northeastern margin of the Tibetan plateau. Tectonics 10 (6), 1091–1110.

Chen, Q., Freymueller, J.T., Wang, Q., Yang, Z., Xu, C., Liu, J., 2004. A deforming block model for the present-day tectonics of Tibet. J. Geophys. Res. 109, B01403.

Chen, Y., Badal, J., Zhang, Z.J., 2009. Radial anisotropy in the crust and upper mantle beneath the Qinghai-Tibet Plateau and surrounding regions. J. Asian Earth Sci. 36, 289–302.

Chen, Y., Badal, J., Hu, J.F., 2010. Love and Rayleigh wave tomography of the Qinghai-Tibet plateau and surrounding areas. Pure Appl. Geophys. 167, 1171–1203.

Cochran, E., Vidale, J., Li, Y.G., 2003. Near-fault anisotropy following the Hector Mine earthquake. J. Geophys. Res. 108 (B9), 2436.

Cochran, E., Li, Y.G., Vidale, J., 2006. Anisotropy in the shallow crust observed around the San Andreas Fault before and after the 2004 M 6.0 Parkfield earthquakes. Bull. Seism. Soc. Am. 96 (4B), S364–S375.

Crampin, S., 1977. A review of the effects of anisotropic layering on the propagation of seismic waves. Geophys. J. R.Astron. Soc. 49, 9–27.

Crampin, S., 1981. A review of wave motion in anisotropic and cracked elastic-media. Wave Motion 3 (4), 343–391.

Crampin, S., Gao, Y., 2018. Evidence supporting new geophysics. Earth and Planetary Physics 2, 173–188. https://doi.org/10.26464/epp2018018.

Crampin, S., Peacock, S., 2005. A review of shear-wave splitting in the compliant crack-critical anisotropic Earth. Wave Motion 41, 59–77.

Crampin, S., Zatsepin, S.V., 1997. Modelling the compliance of crustal rock-II. Response to temporal changes before earthquakes. Geophys. J. Int. 129, 495–506.

Crampin, S., Volti, T., Chastin, S., Gudmundsson, A., Stefánsson, R., 2002. Indication of high pore-fluid pressures in a seismically-active fault zone. Geophys. J. Int. 151, F1–F5.

Deng, Q., Zhang, P., Ran, Y., Yang, X., Min, W., Chu, Q., 2003. Basic characteristics of active tectonics of China. Science in China Ser. D. 46 (4), 356–372 (Chinese Edition).

Fan, J., Li, S., Zhang, X., Liu, M., 2004. Geometric form of Haiyuan fault zone in the crustal interior and dynamics implications. Earthquake Science (Chinese Edition) 17 (1), 43–51.

Gan, W., Zhang, P., Shen, Z.K., Niu, Z., Wang, M., Wan, Y., Zhou, D., Cheng, J., 2007. Present-day crustal motion within the Tibetan Plateau inferred from GPS measurements. J. Geophys. Res. 112, B08416.

Gao, Y., Crampin, S., 2004. Observations of stress relaxation before earthquakes. Geophys. J. Int. 157 (2), 578–582.

Gao, Y., Crampin, S., 2006. A further stress-forecast earthquake (with hindsight), where migration of source earthquakes causes anomalies in shear-wave polarizations. Tectonophysics 426 (3/4), 253–262.

Gao, Y., Wang, P., Zheng, S., Wang, M., Chen, Y., Zhou, H., 1998. Temporal changes in shear wave splitting at an isolated swarm of small earthquakes in 1992 near Dongfang, Hainan Island, southern China. Geophys. J. Int. 135 (1), 102–112.

Gao, Y., Shi, Y.T., Liang, W., Liu, X.Q., Hao, P., 2008. Systematic analysis method of shear-wave splitting SAM (2007) Software system. Earthquake Research China (Chinese Edition) 24, 345–353.

Gao, Y., Wu, J., Yi, G., Shi, Y., 2010. Crust-mantle coupling in North China zone: preliminary analysis from seismic anisotropy. Chin Sci Bull (English Edition) 55 (31), 3599–3605.

Gao, Y., Wu, J., Fukao, Y., Fukao, Y., Shi, Y.T., 2011. Shear-wave splitting in the crust in North China, stress, faults and tectonic implications. Geophys. J. Int. 187 (2), 642–654.

Gao, R., Wang, H.Y., Yin, A., Dong, S.W., Kuang, Z.Y., Andrew, V.Z., Li, W.H., Xiong, X.S., 2013. Tectonic development of the NEern Tibetan Plateau as constrained by high-resolution deep seismic-reflection data. Lithosphere 5, 555–574.

Gao, Y., Shi, Y.T., Chen, A.G., 2018. Crustal seismic anisotropy and compressive stress in the eastern margin of the Tibetan Plateau and the influence of the Ms8.0 Wenchuan earthquake. Chin Sci Bull (Chinese Edition) 63, 1934–1948.

Guo, Z., Chen, Y.J., 2017. Mountain building at northeastern boundary of Tibetan plateau and craton reworking at ordos block from joint inversion of ambient noise tomography and receiver functions. Earth Planet. Sci. Lett. 463, 232–242.

Guo, G.H., Zhang, Z., Cheng, J.W., Dong, Z.P., Yan, J.P., Ma, Y.W., 2015. Seismic anisotropy in the crust in northeast margin of Tibetan plateau and tectonic implication. Chinese J. Geophys. (Chinese Edition) 58 (11), 4092–4105.

Guo, G., Wu, C., Tang, G., Hou, J., Zhang, M., He, Z., Zhang, Z., Pu, J., Liu, X., Chen, J.F., Chen, J.W., 2019. Seismic anisotropy of the northeastern margin of the Tibetan Plateau derived from analysis of SKS and Pms seismic phases. Chinese J. Geophys. (Chinese Edition) 62 (5), 1650–1662.

Huang, Z., Tilmann, F., Xu, M., Wang, L., Ding, Z., Mi, N., Yu, D., Li, H., 2017. Insight into NE Tibetan Plateau expansion from crustal and upper mantle anisotropy revealed by shear-wave splitting. Earth Planet. Sci. Lett. 478, 66–75.

Johnson, J.H., Savage, M.K., Townend, J., 2011. Distinguishing between stress-induced and structural anisotropy at Mount Ruapehu volcano, New Zealand. J. Geophys. Res. 116 (B12), B12303.

Kaneshima, S., 1990. Origin of crustal anisotropy: shear wave splitting studies in Japan. J.

Geophys. Res. 95, 11121–11133.
Kaviris, G., Millas, C., Spingos, I., Kapetanidis, V., Fountoulakis, I., Papadimitriou, P., Voulgaris, N., Makropoulos, K., 2018. Observations of shear-wave splitting parameters in the Western Gulf of Corinth focusing on the 2014 Mw = 5.0 earthquake. Phys. Earth Planet. Inter. 282, 60–76.
Kern, H., Wenk, H.R., 1990. Fabric-related velocity anisotropy and shear wave splitting in rocks from the Santa Rosa Mylonite Zone, California. J. Geophys. Res. 95, 11, 213–11, 224.
Leary, P.C., Crampin, S., McEvilly, T., 1990. Seismic fracture anisotropy in the Earth's crust: an overview. J. Geophys. Res. 95, 11,105–11,114.
Li, Z., Peng, Z., 2017a. Stress- and structure-induced anisotropy in Southern California from two decades of shear wave splitting measurements. Geophys. Res. Lett. 44, 9607–9614.
Li, Z., Peng, Z., 2017b. Two decades of shear-wave splitting measurements in southern California. Geophys. Res. Lett. 44, 9607–9614. https://doi.org/10.1002/2017GL075163.
Li, Y., Wu, Q., Zhang, F., Feng, Q., Zhang, R., 2011. Seismic anisotropy of the Northeastern Tibetan Plateau from shear wave splitting analysis. Earth Planet. Sci. Lett. 304 (1–2), 147–157.
Li, Y.B., Ran, Y.Y., Wang, H., Wu, F.Y., 2016. Paleoseismic records of large earthquakes on the cross-basin fault in the salt lake pull-apart basin and cascade rupture events on the haiyuan fault. Seismology and Geology 38 (4), 830–843.
Li, Y., Pan, J.T., Wu, Q.J., Ding, Z.F., 2017. Lithospheric structure beneath the northeastern Tibetan Plateau and the western Sino-Korea Craton revealed by Rayleigh wave tomography. Geophys. J. Int. 210 (2), 570–584.
Liu, M.J., Li, S.L., Zhang, X.K., Fan, J.C., Song, Z.L., 2004. The observation of trapped waves and the width of the shattered zone in Haiyauan Fault zone. Geophysical & geochemical exploration (in Chinese) 28 (6), 549–552.
Liu, Y., Zhang, H., Thurber, C., Roecker, S., 2008. Shear wave anisotropy in the crust around the San Andreas Fault near Parkfield: spatial and temporal analysis. Geophys. J. Int. 172 (3), 957–970.
Lloyd, G.E., Butler, R.W.H., Casey, M., Mainprice, D., 2009. Mica, deformation fabrics and the seismic properties of the continental crust. Earth Planet. Sci. Lett. 288, 320–328.
Meyer, B., Tapponnier, P., Bourjot, L., Metivier, F., Gaudemer, Y., Peltzer, G., Shunmin, G., Chen, Z., 1998. Crustal thickening in Gansu-Qinghai, lithospheric mantle subduction, and oblique, strike-slip controlled growth of the Tibet Plateau. Geophys. J. Int. 135, 1–47.
Mizuno, T., Ito, H., Kuwahara, Y., Imanishi, K., Takeda, T., 2005. Spatial variation of shear-wave splitting across an active fault and its implication for stress accumulation mechanism of inland earthquakes: the Atotsugawa fault case. Geophys. Res. Lett. 32, L20305.
Müller, M.C., 1991. Prediction of lateral variability in fracture intensity using multi-component shear-wave seismic as precursor to horizontal drilling. Geophys. J. Int. 107, 409–415.
Pan, S., Niu, F., 2011. Large contrasts in crustal structure and composition between the Ordos plateau and the NE Tibetan plateau from receiver function analysis. Earth Planet. Sci. Lett. 303, 291–298.
Peng, Z., Ben-Zion, Y., 2004. Systematic analysis of crustal anisotropy along the Karadere-Duzce branch of the North Anatolian fault. Geophys. J. Int. 159, 253–272.
Qian, Q., Wu, J., Liu, G., Sha, C., Ma, J., Bai, Z., Zhao, Y., Liu, X., 2017. Anisotropy of middle-upper crust derived from shear-wave splitting in the northeastern Tibetan plateau and tectonic implications. Chinese J. Geophys. (Chinese Edition) 60 (6), 2338–2349.
Shapiro, N.M., Ritzwoller, M.H., Molnar, P., Levin, V., 2004. Thinning and flow of Tibetan crust constrained by seismic anisotropy. Science 305 (5681), 233–236.
Shen, Z.K., Wang, M., Li, Y., Jackson, D.D., Yin, A., Dong, D., Fang, P., 2001. Crustal deformation along the Altyn Tagh fault system, western China, from GPS. J. Geophys. Res. 106 (B12), 30607–30621.
Shen, X., Mei, X., Zhang, Y., 2011. The crustal and upper mantle structures beneath the NEern margin of Tibet. Bull. Seismol. Soc. Am. 101 (6), 2782–2795.
Shen, X., Zhou, Y., Zhang, Y.S., Mei, X.P., Guo, X., Liu, X.Z., Qin, M.Z., Wei, C.X., Li, C.Q., 2014. Receiver function structures beneath the deep large faults in the NEern margin of the Tibetan Plateau. Tectonophysics 610, 63–73.
Shen, X., Yuan, X., Liu, M., 2015. Is the Asian lithosphere under thrusting beneath NEern Tibetan Plateau? Insights from seismic receiver functions. Earth Planet. Sci. Lett. 428, 172–180.
Shen, X., Liu, M., Gao, Y., Wang, W., Shi, Y., An, M., Zhang, Y., Liu, X., 2017. Lithospheric structure across the northeastern margin of the Tibetan Plateau: implications for the plateau's lateral growth. Earth Planet. Sci. Lett. 459, 80–92.
Sheng, S.Z., Wan, Y.G., Huang, J.C., Pu, Y.F., Li, X., 2015. Present tectonic stress field in the Circum-Ordos region deduced from composite focal mechanism method. Chinese J. Geophys. (Chinese Edition) 58 (2), 436–452.
Shi, Y.T., Gao, Y., Wu, J., Su, Y.J., 2009. Crustal seismic anisotropy in Yunnan, southwestern China. J. Seism. 13 (2), 287–299.
Shi, Y.T., Gao, Y., Zhang, Y.J., Wang, H., Yao, Z.X., 2013. Shear-wave splitting in the crust in Eastern Songpan-Garzê block, Sichuan-Yunnan block and Western Sichuan Basin. Chinese J. Geophys. (Chinese Edition) 56 (2), 481–494.
Song, Y., Fang, X., Li, J., An, Z., Miao, X., 2001. The Late Cenozoic uplift of the Liupan Shan, China. Science in China, Ser. D. (Chinese Edition) 176-184 (Suppl. 1), 44.
Tai, L.-X., Gao, Y., Shi, Y.-T., Wu, J., 2009. A study of shear-wave splitting in the crust by Liaoning telemetry seismic network of China. Seismology and Geology (Chinese Edition) 31 (3), 401–414.
Tan, J., Li, H., Li, X., Zhou, M., Ouyang, L., Sun, S., Zheng, D., 2015. Radial anisotropy in the crust beneath the northeastern Tibetan plateau from ambient noise tomography. J. Earth Sci. 26 (6), 864–871.
Tian, X.B., Zhang, Z.J., 2013. Bulk crustal properties in NE Tibet and their implications for deformation model. Gondwana Res. 24, 548–559.
Tian, X., Liu, Z., Si, S., Zhang, Z., 2014. The crustal thickness of NE Tibet and its implication for crustal shortening. Tectonophysics 634, 198–207.
Wang, H., Zhang, G., Wang, S., Ma, H., 2004. Stress and strain fields of active tectonic blocks in the China mainland deduced by seismological methods. Chinese J. Geophys. (Chinese Edition) 47 (6), 1164–1174.
Wang, H.Y., Gao, R., Yin, A., Xiong, X.S., Kuang, C.Y., Li, W.H., Huang, W.Y., 2012. Deep structure geometry features of HYFs and deformation of the crust revealed by deep seismic reflection profiling. Chinese J. Geophys. (Chinese Edition) 55 (12), 3902–3909.
Wang, Q., Gao, Y., Shi, Y., Wu, J., 2013. Seismic anisotropy in the uppermost mantle beneath the NEern margin of Tibetan Plateau: evidence from shear wave splitting of SKS, PKS and SKKS. Chinese J. Geophys. (Chinese Edition) 56 (3), 892–905.
Wang, W.T., Zhang, P.Z., Zheng, D.W., Pang, J., 2014. Late Cenozoic tectonic deformation of the Haiyuan fault zone in the northeastern margin of the Tibetan Plateau. Earth Science Frontiers (Chinese Edition) 21 (4), 266–274.
Wang, Q., Niu, F., Gao, Y., Chen, Y.T., 2016. Crustal structure and deformation beneath the NE margin of the Tibetan plateau constrained by teleseismic receiver function data. Geophys. J. Int. 204 (1), 167–179.
Wang, X.C., Ding, Z.F., Wu, Y., Zhu, L.P., 2017. Crustal thicknesses and Poisson's ratios beneath the northern section of the north-south seismic belt and surrounding areas in China. Chinese J. Geophys. (Chinese Edition) 60 (6), 2080–2090.
Wu, Q., Zeng, R., Zhao, W., 2005. The upper mantle structure of the Tibetan Plateau and its implication for the continent-continent collision. Sci. China Ser. D. (Chinese Edition) 48, 1158–1164.
Wu, J., Gao, Y., Chen, Y., 2009. Shear-wave splitting in the crust beneath the southeast Capital area of North China. J. Seismol. 13, 277–286.
Wu, C., Xu, T., Badal, J., Wu, Z., Teng, J., 2015. Seismic anisotropy across the Kunlun fault and their implications for northward transforming lithospheric deformation in northeastern Tibet. Tectonophysics 659, 91–101.
Xiao, Z., Gao, Y., 2017. Crustal velocity structure beneath the northeastern Tibetan plateau and adjacent regions derived from double difference tomography. Chinese J. Geophys. (Chinese Edition) 60 (6), 2213–2225.
Xu, Z., 2001. A present day tectonic stress map for eastern Asia region. Acta Seismologica Sinica (Chinese Edition) 14 (5), 524–533.
Xu, J., Zhao, Z., Ishikawa, Y., 2008. Regional characteristics of crustal stress field and tectonic motions in and around Chinese mainland. Chinese J. Geophys. (Chinese Edition) 51 (3), 770–781.
Xu, X., Niu, F., Ding, Z., Chen, Q., 2018. Complicated crustal deformation beneath the NE margin of the Tibetan plateau and its adjacent areas revealed by multi-station receiver-function gathering. Earth Planet. Sci. Lett. 497, 204–216.
Ye, Z., Gao, R., Li, Q., Zhang, H., Shen, X., Liu, X., Gong, C., 2015. Seismic evidence for the North China plate underthrusting beneath NEern Tibet and its implications for plateau growth. Earth Planet. Sci. Lett. 426, 109–117.
Ye, Z., Li, Q., Gao, R., Zhang, H., Shen, X., Liu, X., Gong, C., 2016. Anisotropic regime across northeastern Tibet and its geodynamic implications. Tectonophysics 671, 1–8.
Yin, A., Rumelhard, P.E., Butler, R., Cowgill, E., Harrison, T.M., Foster, D.A., Ingersoll, R.V., Zhang, Q., Zhou, X., Wang, X., Hanson, A., Raza, A., 2002. Tectonic history of the Altyn Tagh fault system in northern Tibet inferred from Cenozoic sedimentation. Geol. Soc. Am. Bull. 114, 1257–1295.
Yin, A., Dang, Y.Q., Zhang, M., Chen, X.H., Mcrivette, M., 2008. Cenozoic tectonic evolution of the qaidam basin and its surrounding regions (part 3): structural geology, sedimentation, and regional tectonic reconstruction. Geol. Soc. of America Bull. 120 (7-8), 847–876.
Zeng, X.W., Xin, H.L., Chen, C.M., Cai, X.H., 2015. Characteristics research of tectonic stress in southern Ningxia and its adjacent areas by focal mechanisms of small earthquakes. Journal of Seismological Research (Chinese Edition) 38 (1), 51–57.
Zhang, Y., Gao, Y., 2017. The characteristics of crustal shear-wave splitting in North-South seismic zone revealed by near field recordings of two observation periods of ChinArray. Chinese J. Geophys. (Chinese Edition) 60 (6), 2181–2199. https://doi.org/10.6038/cjg20170613.
Zhang, G., Ma, H., Wang, H., Wang, X., 2005. Boundaries between active-tectonic blocks and strong earthquakes in China mainland. Chinese J. Geophys. (Chinese Edition) 48 (3), 662–671.
Zhang, P., Zheng, D., Yin, G., Yuan, D., Zhang, G., Li, C., Wang, Z., 2006. Discussion on Late Cenozoic growth and rise of northeastern margin of the Tibetan Plateau. Quaternary Sciences (Chinese Edition) 26, 5–13.
Zhang, Z., Deng, Y., Teng, J., Wang, C., Gao, R., Chen, Y., Fan, W.M., 2011. An overview of the crustal structure of the Tibetan plateau after 35 years of deep seismic soundings. J. Asian Earth Sci. 40 (4), 977–989.
Zhang, H., Gao, Y., Shi, Y.T., Liu, X.F., Wang, Y.X., 2012a. Tectonics stress analysis based on the crustal seismic anisotropy in the north eastern margin of Tibetan plateau. Chinese J. Geophys. (Chinese Edition) 55 (1), 95–104.
Zhang, H., Teng, J.W., Tian, X.B., Zhang, Z., Gao, R., Liu, J., 2012b. Lithospheric thickness and upper-mantle deformation beneath the NE Tibetan Plateau inferred from S receiver functions and SKS splitting measurements. Geophys. J. Int. 191 (3), 1285–1294.
Zhao, Z.J., Liu, X.J., 1990. Seismic activity and local Tectonics Tress Field in Ningxia and nearby regions. Seismology and Geology (Chinese Edition) 12 (1), 31–46.
Zhao, B., Shi, Y.-T., Gao, Y., 2012. Seismic relocation, focal mechanism and crustal seismic anisotropy associated with the M_S7.1 Yushu earthquake and its aftershocks. Earthq. Sci. 25 (1), 111–119.
Zheng, W., Zhang, P., He, W., Yuan, D., Shao, Y., Zheng, D., Ge, W., Min, W., 2013. Transformation of displacement between strike-slip and crustal shortening in the northern margin of the Tibetan plateau: evidence from decadal GPS measurements and late quaternary slip rates on faults. Tectonophysics 584 (1), 267–280.
Zinke, J.C., Zoback, M.D., 2000. Structure related and stress-induced shear wave velocity anisotropy: observations from microearthquakes near the Calaveras fault in central California. Bull. Seismol. Soc. Am. 90, 1305–1312.